Friction Invariant Object Reconstruction Using a Vibrissa-inspired Tactile Sensor Concept

Lukas Merker
Dept. of Mechanical Engineering
Technische Universität Ilmenau
Ilmenau, Germany
e-mail: lukas.merker@tu-ilmenau.de

Joachim Steigenberger†
Institute of Mathematics
Technische Universität Ilmenau
Ilmenau, Germany

Carsten Behn
Dept. of Mechanical Engineering
Schmalkalden University of Applied Sciences
Schmalkalden, Germany

†*In memory of Univ.-Prof. em. Dr. rer. nat. habil. Joachim Steigenberger (1933–2021).*
We miss his brilliant mind, his warm and humorous manner, his inspiring and constructive personality.

***Abstract*—Vibrissae-inspired sensor concepts hold potential of complementing conventional sensors due to their collision robustness and increased near-field scanning range. In general, they consist of a slender elongated probe, one-sided attached to some kind of measuring device. Making contact with an object, the probe gets bent and transduces (mechanical) signals to its support/the measuring device. Modeling this process analytically, most approaches in literature are based on the assumption of an ideal contact (no stiction or friction). Within the present paper, we extend an existing tactile sensor model for object contour scanning and reconstruction taking first steps to implement frictional effects (Coulomb's law of friction). The probe is modeled as a rod, which is one-sided clamped. Shifting the clamping position relatively to the object of interest, represented by a plane and strictly convex object contour, the rod sweeps along the contour quasi-statically. This process is analyzed in two steps: (1) simulating scanning sweeps in order to generate the support reactions (observables) at the base of the rod theoretically, assuming the object contour and the coefficient of friction to be known, (2) using the generated support reactions from the previous step in order to reconstruct a sequence of contact points, finally approximating the original object contour. Our simulations suggest, that friction affects the observables but (surprisingly) not the actual reconstruction error. Finally, we present a novel approach for reconstructing friction parameters based on the support reactions.**

***Keywords*–Vibrissa; tactile sensor; object scanning; object reconstruction; friction invariance**

I. Introduction

Obstacle avoidance and object identification is a key topic in mobile robotics. Solving these tasks in our everyday life, we humans benefit from our sense of touch complementing visual information. In the same way, robots could benefit from advanced tactile sensors complementing their optical sensors. Beyond the human skin, another prominent natural example functioning as tactile sensors are vibrissae (whiskers) of rodents in animal kingdom. For instance, rats and mice are capable of localizing objects in space based on few vibrissal contacts [1]. As the vibrissal hair-shafts themselves consist of dead tissue, the animals solely rely on the signals sensed by receptors inside the support of each vibrissa, the Follicle-Sinus Complex (FSC) [2]. This biological principle has frequently been transferred to technical sensor concepts [3][4], which basically all share a common structure: a more or less flexible probe, mimicking the vibrissal hair-shaft, one-sided attached to some kind of measuring device, representing the FSC. Making contact with an object of interest, the probe gets bent to varying degrees. Measuring the support reactions (observables) at the base of the rod, conclusions can be drawn about the contact position in space. Ultimately, a whole sequence of contact points can be used to approximate the object's shape [5]. Instead of repeatedly tapping the object of interest with the probe as, e.g., in [6]–[10], one promising scanning strategy is to continuously sweep the probe along the object. The advantage of the sweeping procedure is its passive feasibility [11][12], e.g., using the robot movement as an actuation. Scanning objects via sweeping typically includes large deformations of the probe, whose analysis require nonlinear mechanical models. As such models rarely have solutions expressible in analytical terms, modeling approaches in literature frequently rely on numerics right from the beginning, e.g., [10][12]–[14]. However, these purely numerical approaches share the drawback of missing some important insights and analytical relations of the scanning and reconstruction process. In contrast to these largely numerical models, the authors of [15] presented a continuum model, consisting of a nonlinear Euler-Bernoulli bending rod, whose deformation equations were derived analytically. Using the measured support reactions at the base of the rod, the authors formulated an Initial-Value Problem (IVP). Only at the very end, numerical methods were used to integrate this IVP. In doing so, the contact position along the rod (and finally in space) was determined using a termination condition, that the bending moment at the contact point is zero. A similar model was used in [16] to analyze the problem of object scanning and reconstruction fully analytically in two (inverse) steps:

- step 1 – simulating scanning sweeps in order to generate the support reactions (observables) at the base of the rod theoretically, assuming the object contour to be known, and
- step 2 – using the generated support reactions from the previous step in order to reconstruct a sequence of contact points, finally approximating the original object contour.

Step 2 shows strong similarity to the approach in [15] but

 ISBN: 978-1-61208-882-2

differs by solving the problem fully analytically. Without any demonstration, the author of [16] claimed that the analytical procedure provides the same reconstruction quality as the numerical one used in [15]. However, as [16] is based on the assumption of ideal contacts (no stiction or friction), this statement should be viewed critically and verified using a more realistic contact model. This is where the paper at hand steps in, presenting a preliminary simulation-based study in the development of a more complex analytical vibrissa-inspired sensor model that allows to reconstruct friction and object shape information simultaneously.

The remainder of the paper at hand is structured as follows: In Section II, we present the vibrissa-inspired sensor model deriving the deformation equations of the probe in contact with an object. Following the procedure of [16], we separately analyze the above-mentioned steps 1 and 2 in Section II-A and Section II-B, respectively. Finally, Section III-C presents a novel approach of reconstructing friction parameters during object scanning. In Section III, simulation results are presented and analyzed with the overall goal of verifying some analytical key conditions of [16] in the presence of friction presenting a reconstruction benchmark between [15] and [16]. Finally, the results of the present paper are summed up and some future research subjects are identified in Section IV.

II. MODELING

A single highly flexible probe is modeled as a slender Euler-Bernoulli bending rod of length L consisting of a homogeneous and isotropic material. Its mechanical behavior is basically determined by a constant second moment of area I_z and a constant Young's modulus E. According to [16], we introduce the following units of measure to use only dimensionless system parameters:

$$[length] := L, \quad [force] := \frac{EI_z}{L^2}, \quad [moment] := \frac{EI_z}{L} \quad (1)$$

Considering the rod in a fixed (x, y)-coordinate system, we suppose the lower end of the rod ("foot, base") to be clamped at some point $(x_0, 0)$, see Figure 1. The process of object scanning is considered quasi-statically. It is realized by incrementally shifting the clamping position x_0 (input variable) relative to the object. Consequently, sweeping along the object contour, the rod gets bent and transmits mechanical signals to the clamping. The resulting support reactions f_{0x}, f_{0y} and m_{0z} at the clamping are considered as the observables. The object is assumed as a rigid body with a strictly convex contour function $g : x \mapsto g(x)$. Strict convexity is required for two reasons: Firstly, it prevents simultaneous multi-point contacts between the rod and the object [17]. Secondly, it allows to express the contour function in dependence on its slope angle $\tilde{\alpha} \in [-\frac{\pi}{2}, \frac{\pi}{2}]$ and, thus, we come up with the handy parametrization: $(x, g(x)) \mapsto (\xi(\tilde{\alpha}), \eta(\tilde{\alpha}))$ [16]. In contrast to [16], where the resulting contact force $\vec{f}$ is assumed to be perpendicular to the profile contour tangent, we do not assume such an ideal contact here. Instead, we consider the contact force $\vec{f} = \vec{f}_n + \vec{f}_t$ as composed of a normal component $\vec{f}_n$ and a tangential component $\vec{f}_t$ with the coefficient of friction $\mu = \frac{|\vec{f}_t|}{|\vec{f}_n|} = \tan(\zeta)$, where ζ denotes the friction angle. Then, inspired by Figure 2, the contact force writes:

$$\vec{f} = \vec{f}_n + \vec{f}_t = f[\sin(\alpha)\vec{e}_x - \cos(\alpha)\vec{e}_y] \quad (2)$$

with $\alpha = \tilde{\alpha} + \zeta$.

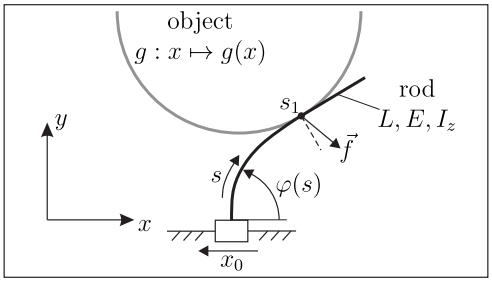

Figure 1. Mechanical model of a rod sweeping along a strictly convex object contour function.

Apart from this, the derivation of the modeling equations describing the elastic line of the rod is fully analogue with [16]. Therefore, it is roughly outlined here: Firstly, the elastic line is parameterized by means of its slope angle φ in dependence on its natural coordinate arc-length $s \in [0, 1]$. Using (2) in order to determine the bending moment $m(s)$, we take advantage of Euler's constitutive law to express the curvature $\kappa(s) = m(s)$ of the elastic line. Finally, introducing an additional differential equation for the curvature, we end up in a system of nonlinear Ordinary Differential Equations (ODEs) of first order:

$$\begin{array}{|ll|ll|} \hline \text{(a)} & x'(s) = \cos(\varphi(s)) & \text{(b)} & y'(s) = \sin(\varphi(s)) \\ \text{(c)} & \varphi'(s) = \kappa(s) & \text{(d)} & \kappa'(s) = f\cos(\varphi(s) - \alpha) \\ \hline \end{array} \quad (3)$$

Remark 1: It is important to understand, that, although (2) *and* (3) *have the same appearence as in [16], the angle $\alpha \geq \tilde{\alpha}$ is defined in a completely different way, no longer representing the slope angle $\tilde{\alpha}$ of the profile contour.*

A. Step 1: generating the support reactions theoretically

For generating the support reactions theoretically, we assume the object contour function as well as the coefficient of friction μ to be known. Within the present paper, we exemplarily consider an object contour function represented by the semi-circle

$$g : x \mapsto g(x) = y_c - \sqrt{r^2 - (x - x_c)^2} \quad (4)$$

with radius r and center coordinates x_c and y_c. During the scanning sweep, a distinction is made between tip and tangential contacts, see Figure 2:

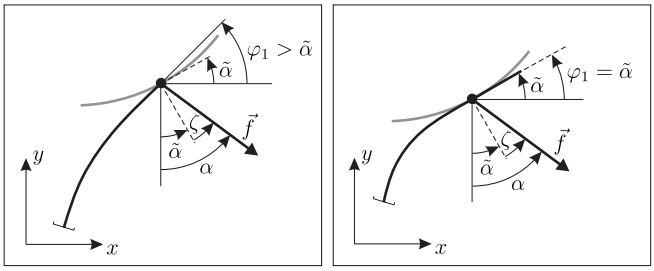

Figure 2. Comparison between (a) tip contact ($s = 1$), and (b) tangential contact ($s = s_1$) with angular relationships.

- For tip contacts, the position of contact along the rod $s_1 = 1$ is known, but the angle $\varphi_1 = \varphi(1) > \tilde{\alpha}$ is unknown
- In turn, for tangential contacts, the position of contact along the rod s_1 is unknown, but instead, we have the angular relationship $\varphi = \tilde{\alpha}$.

Finally, these observations result in the following Boundary-Conditions (BCs) at the clamping (5), for tip (6) and tangential contacts (7):

$$\boxed{\begin{array}{ll}\text{(a)}\ \ x(0) = x_0 & \text{(b)}\ \ y(0) = 0 \\ \text{(c)}\ \ \varphi(0) = \dfrac{\pi}{2} & \text{(d)}\ \ \kappa(0) = \kappa_0\end{array}} \tag{5}$$

$$\boxed{\begin{array}{ll}\text{(a)}\ \ x(1) = \xi(\tilde{\alpha}) & \text{(b)}\ \ y(1) = \eta(\tilde{\alpha}) \\ & \text{(c)}\ \ \kappa(1) = 0\end{array}} \tag{6}$$

$$\boxed{\begin{array}{ll}\text{(a)}\ \ x(s_1) = \xi(\tilde{\alpha}) & \text{(b)}\ \ y(s_1) = \eta(\tilde{\alpha}) \\ \text{(c)}\ \ \varphi(s_1) = \tilde{\alpha} & \text{(d)}\ \ \kappa(s_1) = 0\end{array}} \tag{7}$$

Remark 2: It is important to note, that (via α) ζ does affect the ODE system (3)*, but not the BCs* (6) *and* (7)*, see Figure 2. Instead, the BCs solely depend on the object slope $\tilde{\alpha}$.*

The process of generating the observables is realized by simulating scanning sweeps in Matlab 2019a. In doing so, the two-point boundary-value problems (3)&(5)&(6) and (3)&(5)&(7) are solved using shooting methods to determine the unknown parameters f_1, α, κ_0 and s_1. Finally, having the mentioned parameters at hand, the support reactions are determined in the following way:

$$f_{0x} = -f\sin(\alpha), \qquad f_{0y} = f\cos(\alpha), \qquad m_{0z} = -\kappa_0 \tag{8}$$

B. Step 2: Reconstructing contact points

For reconstructing a sequence of contact points, we assume the support reactions f_{0x}, f_{0y}, m_{0z} and the clamping position x_0 to be known in advance, either from step 1 or from measurements using a real experimental setup. Consequently, the unknown parameters f, α and κ_0 are determined evaluating (8) in the following way:

$$f = \sqrt{f_{0x}^2 + f_{0y}^2}, \quad \alpha = -\arctan\left(\frac{f_{0x}}{f_{0y}}\right), \quad \kappa_0 = -m_{0z} \tag{9}$$

Note, as α is not necessarily restricted to the domain $[-\frac{\pi}{2}, \frac{\pi}{2}]$ as in [16], the four-quadrant inverse tangent atan2 must be used in (9). Now, having all parameters of (5) at hand, we consider the IVP (3)&(5). As mentioned in Section I, the integration of this IVP can be realized numerically as in [15] or analytically as in [16]:

- In [15], a termination condition is used which cancels the numerical integration, if $\kappa(s_1) = m(s_1) = 0$ is fulfilled.
- In [16], the position s_1 is determined by solving the analytic expression using elliptic integrals

$$s_1 = -\frac{1}{\sqrt{2f}} \int_{\frac{\pi}{2}}^{\tilde{\alpha}} \frac{1}{\sqrt{\sin(t - \tilde{\alpha})}} dt \tag{10}$$

Both procedures (even the analytical derivation of (10)) are based on the fact, that the curvature at s_1 is zero. Therefore, it can be expected, that both procedures lead to the same results (except for minor numerical deviations). In fact, this hypothesis was made in [16], but without any proof or demonstration. Within the present paper, we take advantage of both reconstruction procedures comparing their results in a benchmark with a surprising result in Section III.

C. Reconstructing friction parameters

Assuming an ideal contact ($\zeta = 0 \Rightarrow \alpha = \tilde{\alpha}$) in [16], the problem of reconstructing the object slope $\tilde{\alpha}$ was trivial, as it was simply determined by the support reactions using (9). In the same way we are able to determine the orientation α of the contact force $\vec{f}$. However, here we face the problem that $\alpha = \tilde{\alpha} + \zeta$ includes two components – the object slope $\tilde{\alpha}$ and the friction angle ζ, see Figure 2. Without knowing the friction coefficient, it seems impossible, to separate α in its components. Adressing this problem, we use the curvature ODE (3)(d) together with (7)(d) to formulate the first integral

$$\frac{1}{2}\kappa(s)^2 = f(\varphi(s) - \alpha) - f(\varphi_1 - \alpha) \tag{11}$$

where $\varphi(s_1) = \varphi_1$. Now, substituting $s = 0$ and solving for φ_1 yields

$$\varphi_1 = \alpha - \arcsin\left(\frac{m_{0z}^2 - 2f_{0y}}{2f}\right) \tag{12}$$

$$= \tilde{\alpha} + \zeta - \beta \tag{13}$$

with $\beta := \arcsin\left(\frac{m_{0z}^2 - 2f_{0y}}{2f}\right)$. Analyzing (13), we again distinguish between tip and tangential contacts, see Figure 2:

- For tip contacts ($\varphi_1 > \tilde{\alpha}$), it can merely be concluded that $\beta < \zeta$.
- In contrast, for tangential contacts ($\varphi_1 = \tilde{\alpha}$), (13) can be rewritten in the following way:

$$\boxed{\zeta = \beta = \arcsin\left(\frac{m_{0z}^2 - 2f_{0y}}{2f}\right)} \tag{14}$$

Thus, in case of tangential contact, both the friction angle ζ and the coefficient of friction $\mu = \tan(\zeta)$ are determinable based on the support reactions. Then, the object slope is $\tilde{\alpha} = \alpha - \zeta$ and $\vec{f}$ decomposes into

$$\begin{aligned}\vec{f}_n &= f\cos(\zeta)\left[\sin(\tilde{\alpha})\,\vec{e}_x - \cos(\tilde{\alpha})\,\vec{e}_y\right] \\ \vec{f}_t &= f\sin(\zeta)\left[\cos(\tilde{\alpha})\,\vec{e}_x + \sin(\tilde{\alpha})\,\vec{e}_y\right]\end{aligned} \tag{15}$$

III. Results and Discussion

A. Generating the support reactions

Figure 3a shows an exemplary simulated scanning sweep of the rod along the circular object contour (4) with $r = 0.9$, $x_c = 0$ and $y_c = 1.3$ from right to left (negative x-direction). The sweep is represented by a sequence of elastic lines (equilibrium states), where tip contacts are colored in blue and tangential ones in red for $s \in (0, s_1)$ and black for $s \in (s_1, 1)$. The scanning sweep aborts at some point, where the rod would detatch from the object (snap-off). In general, the appearance

of Figure 3a does not change significantly with varying μ. Therefore, in Figure 3a we limit ourselves to only one example with $\mu = 0$. In Figs. 3b-3d, the support reactions f_{0x}, f_{0y} and m_{0z} for scanning sweeps with different friction coefficients $\mu = 0.0 : 0.2 : 0.6$ are plotted against the clamping position x_0. Additionally, the gray curve in each figure represents the support reactions resulting from a scanning sweep with a uniformly distributed random friction coefficient. In doing so, a random value $\mu \in [0, 0.4]$ was generated for each clamping position x_0 in order to model friction parameter uncertainty. In Figs. 3b-3d, the transitions between tip and tangential contacts (see Figure 3a) and vice versa are marked with a small circle. Note, that all Figs. 3a-3d are to be read from right to left, due to the scanning direction.

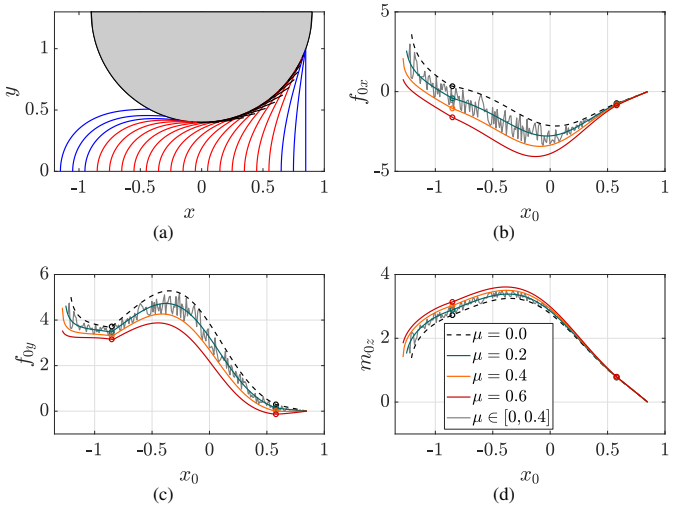

Figure 3. Object scanning: (a) sequence of equilibrium states during a scanning sweep (from right to left) along a circular object contour; (b)-(d) support reactions (observables) f_{0x}, f_{0y} and m_{0z} in dependence on different friction coefficients μ including a uniformly distributed random $\mu \in [0, 0.4]$ (gray line).

Based on Figure 3, we highlight the following observations:

- All support reactions are affected by the friction coefficient μ. For instance, the clamping moment m_{0z} consistently increases with increasing μ.
- Moreover, an increasing coefficient μ results in a longer overall contact phase, which is apparent comparing the values of x_0 at the end of each scanning sweep (left side of each curve).
- The friction coefficient μ has little impact on the transitions between tip and tangential contacts.

Summarizing, the simulation of step 1 allows for the generation of the support reactions in dependence on a pre-set (known) friction coefficient. Note that adjusting the friction coefficient to a defined value (as in the simulation) would be difficult to realize in an experiment. This highlights the actual importance of simulation step 1. Now, having the support reactions based on different friction coefficients μ at hand, this enables a comprehensive investigation of step 2. In the following, a comparison is made for the reconstruction procedures of [15] and [16] (see Section II-B) based on the support reactions in Figure 3b-3d.

B. Benchmark: Reconstructing contact points

As discussed in Section II, the basis for reconstructing contact points in space is the determination of the contact location s_1 along the rod. Here, we compare the approaches of [15] and [16] (see Section II), starting with an evaluation of s_1 in Figs. 4a and 4b. In Figure 4a, s_1 is determined based on [15] using an event-function, which cancels the numerical integration, when the curvature of the rod is zero for the first time. It is obvious, that all curves $s_1(x_0)$ are quite close to each other, and therefore, the friction coefficient seems to have little impact on s_1 during object scanning: the enlarged section shows, that an increasing friction coefficient generally results in a slightly larger s_1. By analogy with Figs. 3b-3c, the gray curve of s_1, resulting from a random friction coefficient, oscillates between the orange and the black one.

In Figure 4b, s_1 is determined based on [16]. Evaluating the support reactions using (10), two main observations were made:

- Considering the case $\mu = 0$ (black curve), the fact that (10) returns values larger than 1 in the presense of tip contacts, as stated in [16], is correct for a large extend of the scanning sweep. Note that all values exceeding 1 are replaced by the value $s_1 = 1$ (tip of the rod) in Figure 4b. However, one exception, where (10) returns values lower than 1, even though the rod is in tip contact, is observed at the very end of the scanning sweep (see black curve in Figure 4b). Hence, using (10) as a decision criterion between tip and tangential contact is not adequate.
- For $\mu > 0$, (10) does no longer provide any information about the contact phase at all, see Figure 4b. Moreover, from a certain threshold (in our case $\mu \geq 0.4$), the arguments exceed the definition range of (10) for some clamping positions x_0. For instance, the orange and red curves are not defined at the beginning of the scanning sweep, see Figure 4b.

Comparing Figs. 4a and 4b it is obvious, that, in the absence of friction (black curves), the reconstructed contact positions s_1 along the rod are almost identical. However, there seems to be a huge difference in the reconstruction procedures of [15] and [16], which only becomes noticeable in the presense of friction. The origin of this difference lies in the derivation of the analytical condition (10). There, the condition $\varphi = \alpha$ is used assuming an ideal, tangential contact. And exactly that is the problem: The condition $\varphi = \tilde{\alpha} = \alpha$ is indeed valid for the case $\mu = 0$ (ideal contact), but results in increasing errors with increasing μ: $\varphi = \tilde{\alpha} = \alpha - \mu$. In contrast, the reconstruction procedure of [15] dispenses with the mentioned geometric condition. Therefore, it is not affected by increasing friction coefficients. Note that the slight deviations in Figure 4a are not caused by any reconstruction error, but instead they reflect the actual change of s_1 caused the change of μ. Beyond the contact position s_1, the actual reconstructed sequences of contact points are shown in Figs. 4c and 4d. Again, Figure 4c is based on the reconstruction procedure presented in [15] while Figure 4d is based on [16]. In both cases, the reconstructed sequences of contact points are superimposed by the original object contour (gray line). The corresponding reconstruction

 ISBN: 978-1-61208-882-2

errors, which are defined as the smallest (perpendicular) distance to the original object contour, are indicated in Figs. 4e and 4f.

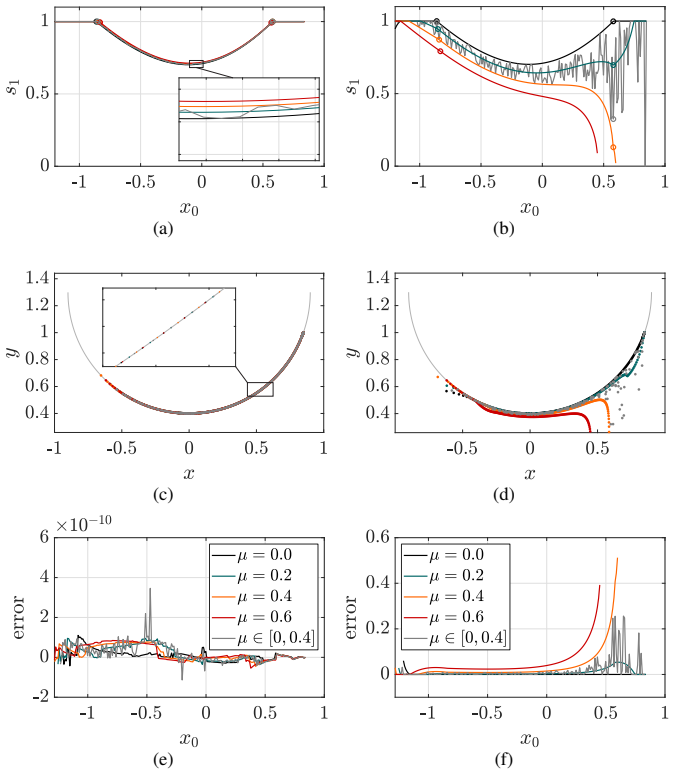

Figure 4. Object reconstruction using the support reactions (observables) from Figs. 3b–3d: (a) reconstruction of s_1 based on [15]; (b) reconstruction of s_1 using (10) based on [16]; (c) reconstructed contact points based on [15]; (d) reconstructed contact points based on [16]; (e) reconstruction error corresponding to (c); (f) reconstruction error corresponding to (d).

The following two observations must be highlighted:

- Most noteworthy, independently on μ, the reconstructed contact points using the procedure of [15] lie exactly on the original object contour, see enlarged section of Figure 4c. This fact reflects in Figure 4e, where the reconstruction errors are within numerical boundaries for all friction coefficients μ, including the randomly generated one. This is probably the most important observation of the presented paper. With increasing μ, the reconstructed contact points shift along the object contour while the reconstruction error remains unchanged. This is what we refer to as friction invariant reconstruction.
- In contrast, the reconstructed points in Figure 4d are characterized by larger errors. For $\mu = 0$, the reconstruction error in Figure 4d (black line) is in the same order of magnitude as those in Figure 4c, except for the end of the scanning sweep. In general, the reconstruction error increases with increasing friction coefficient μ. The reconstruction based on the randomly generated μ is characterized by many outliers. Summarizing, being not friction invariant, the reconstruction error of s_1, see Figure 4b, reappears in the reconstruction of the contact points in Figure 4d.

C. Reconstructing friction parameters

Besides the reconstructed contact points, it can be advantageous in many ways to know the normal direction of an object – on the one hand, normal directions might assist in fitting a curve through he reconstructed contact points, improving the reconstruction quality. On the other hand, they might be evaluated for object manipulation, e.g., grasping. In the following, we use the observables from Figs. 3b–3d in order to verify the analytical condition (14). The angle $\beta = \alpha - \varphi_1$, see (12), is plotted against the clamping position x_0 in Figure 5a, where the phase transitions are indicated by circular markers. According to Section II, the condition $\beta = \zeta$ holds in case of tangential contact, i.e., in the interval enclosed by the markers in Fig. 5a, where the angle β is constant. In order to evaluate the data, the coefficient of friction $\mu = \tan(\zeta)$ is determined based on the reconstructed friction angle ζ. For the tangential contact phase, $\mu(x_0)$ is shown in Fig. 5b.

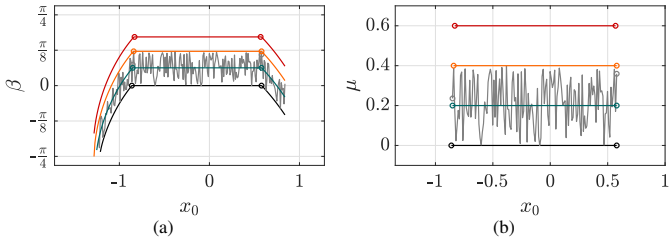

Figure 5. Reconstructing friction parameters: (a) angle $\beta = \alpha - \varphi_1$ plotted against the clamping position x_0 (phase transitions marked with circles); (b) friction coefficient $\mu = \tan(\zeta)$ for tangential contacts.

It can be seen that the reconstructed friction coefficients are consistent with the values originally assumed for μ. Even the noisy function for $\mu \in [0, 0.4]$ matches the pre-set one in simulation step 1. The observation confirms the hypothesis that, for tangential contacts, the contact force $\vec{f}$ can be decomposed into its normal and tangential components by means of (15), see Section II.

IV. Conclusion

The paper at hand presented a mechanical model of a vibrissa-inspired tactile sensor for object contour scanning and reconstruction in the presence of Coulomb friction. In doing so, two different processes were analyzed separately: Firstly, scanning sweeps along a known object contour assuming a pre-set friction coefficient were simulated in order to generate the support reactions (observables) theoretically. Afterwards, these support reactions were used in order to reconstruct a sequence of contact points. In doing so, the reconstruction approaches of [15] and [16] were compared in a benchmark test. Finally, a novel approach of determining friction parameters based on the support reactions was presented, resulting in a handy analytical expression. Summarizing the results of the paper at hand, we highlight the following observations: During object scanning, dry friction affects the support reactions. It turned out that the reconstruction approach presented in [15] is friction invariant, i.e., friction does not affect the reconstruction error. In contrast, the approach presented in [16] is applicable just as well as the one presented in [15] in the absence of friction, but results in large reconstruction errors in the presence of friction.

 ISBN: 978-1-61208-882-2

However, even though the approach in [16] is not friction invariant, it laid an important foundation for all investigations of the present paper. By identifying the essential differences between the mentioned two approaches, it is expected that the analytical conditions from [16] can be adapted in future work to be friction invariant as well. Finally, the novel approach of detecting friction parameters based on the support reactions was verified by simulations.

The mentioned findings suggest that the presented measuring principle is highly suitable to complement optical sensors in robot exploration and path planning tasks. For instance, a robot equipped with one (or multiple) vibrissa-like sensors might move through the environment, passively dragging the highly flexible probe. After accidentally making a soft contact between some point of the probe and an object/obstacle in the environment, the probe would get bent, causing the support reactions to exceed a certain activation threshold. Subsequently, the measured signals might be used to draw further conclusions about the object's shape and ultimately to assist in path-planning algorithms, tracking a prescribed value of the support reactions to achieve an optimal scanning movement of the robot, relative to the object.

The research conducted in this paper is particularly limited by the use of a quasi-static model. Against this background, only static friction but no dynamical effects, e.g., stick-slip effects can be discussed. However, the fact that even a randomly generated (noisy) friction coefficient did not invalidate the investigations suggests, that the results in the paper at hand also apply to practical scenarios. Finally, it remains to verify the theoretical results on practical examples by using an experimental setup which has already been attacked in the first steps.

REFERENCES

[1] T. J. Prescott, B. Mitchinson, and R. A. Grant, "Vibrissal behavior and function," Scholarpedia, vol. 6, pp. 6642, 2011.

[2] S. Ebara, T. Furuta, and K. Kumamoto, "Vibrissal mechanoreceptors," Scholarpedia, vol. 12, pp. 32372, 2017.

[3] F. A. Lucianna, A. L. Albarracín, S. M. Vrech, F. D. Farfán, and C. J. Felice, "The mathematical whisker: A review of numerical models of the rat's vibrissa biomechanics," J. Biomech., vol. 49, pp. 2007–2014, 2016.

[4] C. Behn, "Mathematical Modeling and Control of Biologically Inspired Uncertain Motion Systems with Adaptive Features," Habilitation, Technische Universität Ilmenau, Germany, 2013.

[5] C. L. Schroeder and M. J. Z. Hartmann, "Sensory prediction on a whiskered robot: a tactile analogy to optical flow," Frontiers in Neurorobotics, vol. 6, 2012. DOI: 10.3389/fnbot.2012.00009.

[6] T. Tsujimura and T. Yabuta, "Object detection by tactile sensing method employing force/torque information," IEEE Trans. Robot. Autom., vol. 5, pp. 444–450, 1989.

[7] M. Kaneko, N. Kanayama, and T. Tsuji, "Active antenna for contact sensing," IEEE Trans. Robot. Autom., vol. 14, pp. 278–291, 1998.

[8] J. H. Solomon and M. J. Z. Hartmann, "Artificial whiskers suitable for array implementation: Accounting for lateral slip and surface friction," IEEE Trans. Robot., vol. 24, pp. 1157–1167, 2008.

[9] J. A. Birdwell et al., "Biomechanical models for radial distance determination by the rat vibrissal system," J. Neurophysiol., vol. 98, pp. 2439–2455, 2007.

[10] D. Kim and R. Möller, "Biomimetic whiskers for shape recognition," Robot. Auton. Syst., vol. 55, pp. 229–243, 2007.

[11] L. Merker, J. Steigenberger, R. Marangoni, and C. Behn, "A vibrissa-inspired highly flexible tactile sensor: scanning 3D object surfaces providing tactile images," Sensors, vol. 21, 2021. DOI: 10.3390/s21051572.

[12] J. H. Solomon and M. J. Z. Hartmann, "Extracting object contours with the sweep of a robotic whisker using torque information," Int. J. Robot Res., vol. 29, pp. 1233–1245, 2010.

[13] B. W. Quist, R. A. Faruqi, and M. J. Z. Hartmann, "Variation in Young's modulus along the length of a rat vibrissa," Journal of Biomechanics, vol. 44, pp. 2775–2781, 2011.

[14] L. A. Huet, J. W. Rudnicki, and M. J. Z. Hartmann, "Tactile sensing with whiskers of various shapes: determining the three-dimensional location of object contact based on mechanical signals at the whisker base," Soft Robotics, vol. 4, pp. 88–102, 2017.

[15] G. R. Scholz and C. D. Rahn, "Profile sensing with an actuated whisker," IEEE Trans. Rob. Autom., vol. 20, pp. 124–127, 2004.

[16] C. Will, "Continuum Models for Biologically Inspired Tactile Sensors: Theory, Numerics and Experiments," Ph.D. Thesis, Technische Universität Ilmenau, Germany, 2018.

[17] L. Merker, S. J. Fischer Calderon, M. Scharff, J. H. A. Miranda, and C. Behn, "Effects of Multi-Point Contacts during Object Contour Scanning Using a Biologically-Inspired Tactile Sensor," Sensors, vol. 20, 2020. DOI: 10.3390/s20072077.

 ISBN: 978-1-61208-882-2